Secondary-electron emission by MeV He ions reflected from a SnTe(001) surface: Separation of above- and below-surface processes

Kimura, K; Ooki, S; Andou, G; Nakajima, K

PHYSICAL REVIEW A, VOLUME 61, 012901

Secondary-electron emission by MeV He ions reflected from a SnTe(001) surface: Separation of above- and below-surface processes

Kenji Kimura,* Suguru Ooki, Gou Andou, and Kaoru Nakajima
Department of Engineering Physics and Mechanics, Kyoto University, Kyoto 606-8501, Japan
(Received 27 May 1999; published 8 December 1999)

We have measured the secondary-electron (SE) yield in coincidence with 1–2-MeV $He^{+,2+}$ ions reflected from a SnTe(001) at grazing incidence. Specific ion trajectories, i.e., true specular reflection and subsurface channeling, can be distinguished in the energy spectrum of the reflected ions. By selecting the specific trajectories, above- and below-surface SE production processes are separately studied. The position-dependent SE production rate for 2-MeV He^{2+} is found to be about four times larger than that for 0.5-MeV H^+, indicating that the SE production rate at the surface is proportional to q^2. Analyzing the SE number distributions for subsurface channeled ions, the mean free path of SE's in SnTe is estimated to be 0.6 nm.

PACS number(s): 34.50.Dy, 79.20.−m, 61.85.+p, 79.60.Bm

I. INTRODUCTION

Secondary-electron (SE) emission induced by ion impact is one of the most fundamental phenomena in ion-solid interactions [1]. It has been studied for a long time not only from the viewpoint of fundamental physics but also for practical reasons in many applications, such as particle detectors, plasma-wall interactions, and ion microcopy. The mechanism of the SE emission is usually understood by a so-called ''three-step model'' [2]. The three steps are production of the excited electrons in the solid, transport to the surface, and transmission through the surface barrier. For the ion velocities larger than about 10^7 cm/s, the dominant production process is the kinetic electron emission (KEE) [3]. The SE production rate for KEE was believed to be proportional to the electronic stopping power S_e because the observed SE yield γ is roughly proportional to S_e [2,3]. Recently, we have demonstrated that the production process can be observed separately from other processes utilizing the specular reflection of fast ions, and found that the position-dependent SE production rate is not proportional to the position-dependent stopping power [4]. The observed SE production rate was explained in terms of a direct excitation process as well as decay of plasmons into electron-hole pairs [4]. In addition, unexpected enhancement of the SE emission in front of insulator surfaces was observed, which was attributed in part to a large conversion probability of the excited surface plasmons into electron-hole pairs [5]. Thus, the SE production process at the surface is clear, but other processes, i.e., the transport and transmission processes, are still left for further investigation. In the present paper, we demonstrate that above- and below-surface SE production processes can be separately observed by selecting specific ion trajectories in the energy spectrum of the scattered ions. Using this separation, the escape process of the SE's produced inside solids is studied.

*Author to whom correspondence should be addressed. FAX: +81-75-753-5253. Electronic address: kimura@kues.kyoto-u.ac.jp

II. EXPERIMENT

Details of the experimental procedure are described elsewhere [4]. Briefly, a single crystal of SnTe(001) was prepared by epitaxial growth *in situ* by vacuum evaporation on a cleaved surface of KCl at 250 °C in an ultrahigh-vacuum chamber. The crystal was mounted on a five axis precision goniometer. Beams of 1–2-MeV $He^{+,2+}$ ions from the 1.7-MV Tandetron accelerator of Kyoto University were collimated by a series of apertures to less than $0.1\times0.1\,mm^2$ and to a divergence angle less than 0.3 mrad. The collimated ion beams were incident on the SnTe(001) at glancing angles $\theta_i=2-7$ mrad. The ions are reflected from the surface at the specular angle without penetration inside the crystal unless they hit a surface step [6]. The azimuthal angle of the crystal was carefully chosen to avoid surface axial channeling. The ions scattered at the specular angle were selected by an aperture ($\phi=1$ mm) placed 425 mm downstream from the target and energy analyzed by a 90° sector magnetic spectrometer.

Secondary electrons emitted from the target crystal were detected by a microchannel plate (MCP, effective diameter $\phi=20$ mm) placed in front of the target. The MCP was biased at +700 V to collect all SE's emitted from the target. The pulse height, I, of the MCP signal is proportional to the number of SE's detected [7]. In order to convert the pulse height into the number, N_e, of SE's emitted, we used the SE yields measured with a conventional current method in a previous study [8].

III. RESULTS AND DISCUSSION

An example of the observed energy spectrum of 2-MeV He^{2+} ions reflected from the SnTe(001) is shown in Fig. 1. Besides a main peak at ~1980 keV (referred to as the first peak), which corresponds to the specularly reflected ions, there are additional small peaks at ~1940 and ~1900 keV. These peaks are referred to as the second and third peaks hereafter. The second (third) peak corresponds to the ions which penetrate inside the crystal through surface steps and appear again after channeling through the crystal for one (two) wavelength(s) of the channeling motion, as shown in

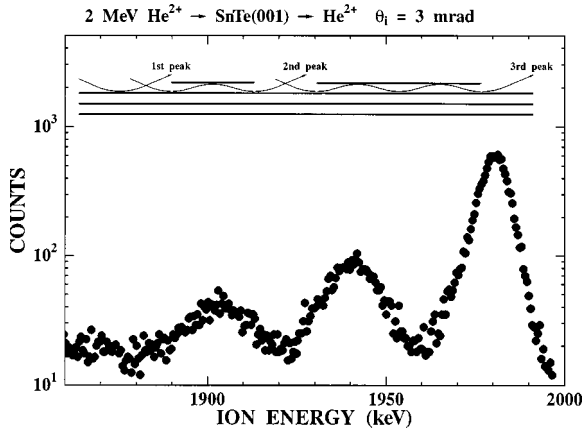

FIG. 1. Energy spectrum of He^{2+} ions specularly reflected from SnTe(001) when 2-MeV He^{2+} ions are incident at $\theta_i = 3$ mrad. The first peak at ~1980 keV corresponds to the ions reflected without penetration into the crystal, and the small peaks at ~1940 and ~1900 keV correspond to the subsurface channeled ions as shown by the inset.

the inset [6]. These ions are called subsurface channeled ions. The energy loss of the second (third) peak ion is about three (five) times larger than that of the first peak ion because the second (third) peak ion is deflected by the atomic plane three (five) times while the first peak ion is deflected once. First, we will concentrate on the SE's emitted by the first peak ions.

A. Above-surface process

Figure 2 displays examples of the observed pulse-height distributions of the MCP signals at incidence of 1-MeV He^+ ions with $\theta_i = 4$ mrad. The abscissa shows the number of SE's. The result of a noncoincidence measurement is shown together with the pulse-height distributions measured in coincidence with the reflected He^+ and He^{2+} ions of the first peak. The coincidence spectrum shows a well-defined peak and the mean SE number (SE yield) for He^{2+} ($\gamma = 186$) is

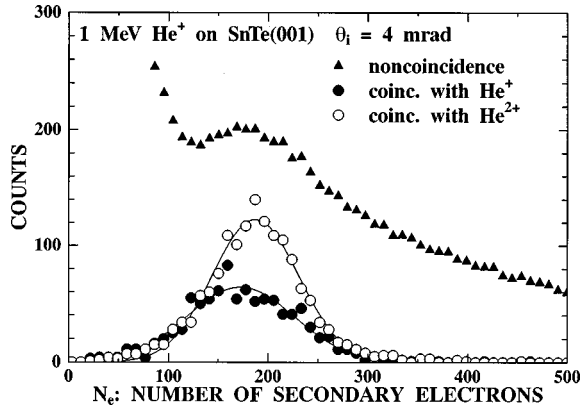

FIG. 2. Pulse-height distributions of secondary electrons detected by MCP when 1-MeV He^+ ions are incident on SnTe(001) at $\theta_i = 4$ mrad. The triangles show the noncoincidence result and the closed (open) circles show the distribution measured in coincidence with the reflected He^+ (He^{2+}) ions of the first peak.

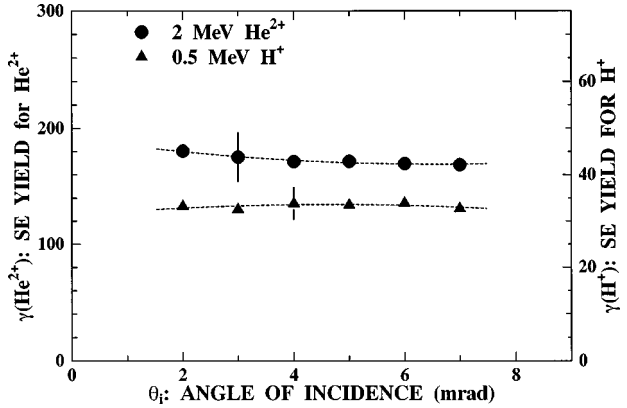

FIG. 3. Secondary-electron yields induced by 2-MeV He^{2+} (circle) and 0.5-MeV H^+ ions (triangle) specularly reflected from the SnTe(001) as a function of the angle of incidence.

slightly higher than that for He^+ ($\gamma = 174$), indicating that the reflected He^{2+} ion emits more electrons than He^+. Although the SE yield is expected to be proportional to q^2, the observed yield for He^{2+} is larger than that for He^+ by only several %. This indicates that the reflected ion is subject to frequent charge-exchange processes in the vicinity of the surface [9]. As a result, the difference of the charge state in the last part of the outgoing trajectory is responsible for the observed small difference of the SE yields.

Figure 3 displays an example of the SE yield measured in coincidence with the reflected He^{2+} ions when 2-MeV He^{2+} ions were incident on the SnTe(001). The result for 0.5-MeV H^+, which has the same velocity as 2-MeV He, is also shown for comparison. The observed He^{2+} fraction of the reflected ions was about 96% at 2 MeV irrespective of the incident charge state [10] and the H^+ fraction was larger than 99% at 0.5 MeV. The effective charge for the specularly reflected 2-MeV He ion is estimated as $q_{\mathrm{eff}}^2 = 0.96 \times 2^2 + 0.04 \times 1^2 = 3.88$. The SE yield for He^{2+} is, however, five to six times larger than that for H^+, suggesting that the SE production rate increases more rapidly than q_{eff}^2. A detailed analysis is required before concluding the steep q_{eff} dependence of the production rate because the ion trajectories for He^{2+} and H^+ might be different.

In the previous study, we have shown that the position-dependent SE production rate $P(x)$ can be derived from the observed $\gamma(\theta_i)$,

$$P(x) = -\frac{1}{2\pi E}\frac{dV(x)}{dx}\left(\gamma(0)\left(\frac{E}{V(x)}\right)^{1/2} + \int_0^{\pi/2}\left.\frac{d\gamma(\beta_i)}{d\theta_i}\right|_{\theta_i=\sqrt{[V(x)/E]}\sin(u)} du\right), \quad (1)$$

where $V(x)$ is the surface continuum potential and E the ion energy [4]. We use the universal potential with a screening distance $a_U = 0.885\,34 a_B (Z_1^{0.23} + Z_2^{0.23})^{-1}$ for $V(x)$ [11]. The result for 2-MeV He^{2+} at the SnTe(001) is shown together with the previous result for 0.5-MeV H^+ [4] in Fig. 4. The

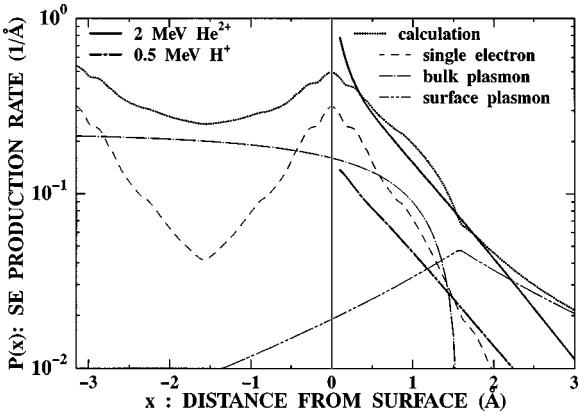

FIG. 4. Position-dependent secondary-electron production rates for 0.5-MeV H^+ (thick dot-dashed curve) and 2-MeV He^{2+} ions (solid curve). Calculated production rates for the single-electron process (dashed curve), bulk-plasmon-assisted process (dot-dashed curve), surface-plasmon-assisted process (double-dot-dashed curve), and the sum of them (dotted curve) are also shown for 2-MeV He^{2+}.

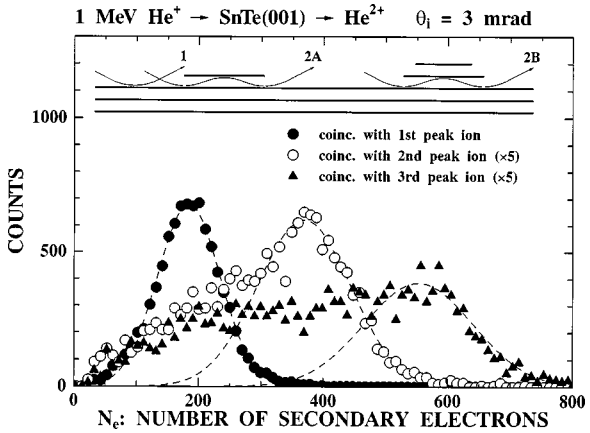

FIG. 5. Pulse-height distributions of the MCP signal when 1-MeV He^+ ions are incident on the SnTe(001) at $\theta_i = 3$ mrad. The distribution measured in coincidence with the reflected He^{2+} ions of the first peak (closed circle), that of the second peak (open circle), and that of the third peak (triangle) are shown. The inset shows examples of the ion trajectories of the first peak ions (labeled 1) and the second peak ions ($2A$ and $2B$).

derived $P(x)$ for He^{2+} is about four times larger than that for H^+, indicating that the SE production rate is proportional to q_{eff}^2.

The dominant mechanisms of the SE production are the direct excitation by single collision and the plasmon-assisted process in the present case. The number of electrons directly excited over the vacuum level by ion impact can be calculated with the binary encounter model [4]. We assumed that half of the excited electrons are ejected into vacuum and others are impinged into the solid. The calculated result is shown by a dashed curve in Fig. 4. Concerning the plasmon-assisted process, the surface stopping power for charged particles due to surface plasmon excitation was first studied by Echenique and Pendry [12]. Kawai *et al.* derived formulas of the surface- and bulk-plasmon excitation probabilities by fast ions traveling at surfaces [13]. the SE production rates for the bulk- and surface-plasmon-assisted processes were calculated with their formulas. In the calculation, the bulk-plasmon energy of 14 eV is employed and the conversion efficiency of plasmons into electron-hole pairs is assumed to be 100% for bulk plasmons and 30% for surface plasmons, which was determined in the previous study of H^+ impact on SnTe(001) [4]. The calculated results are shown by a dot-dashed and a double-dot-dashed curve, respectively. The sum of these three contributions (single collision, bulk-, and surface-plasmon-assisted processes) is shown by a dotted curve, which agrees roughly with the experimental result. The production rate inside the crystal was also calculated and shown in Fig. 4. Note that the bulk-plasmon-assisted process is dominant inside the crystal. The calculated production rate will be used in the discussion on the below-surface process.

B. Below-surface process

Figure 5 shows the MCP pulse-height distributions measured in coincidence with the He^{2+} ions of the first, second, and third peaks when 1-MeV He^+ ions are incident at $\theta_i = 3$ mrad. The average SE yields calculated from the observed distributions are $\gamma_1 = 183$, $\gamma_2 = 310$, and $\gamma_3 = 406$ for the first, second, and third peak ions, respectively. Although the energy losses of the second and third peak ions are three and five times larger than that of the first peak ion (see Fig. 1), the corresponding SE yields are only 1.7 and 2.2 times larger than that of the first peak ion. This is because the electrons excited by the subsurface channeled ions inside the crystal are subject to the transport and transmission processes and so only a part of them can appear as SE's.

Looking at the SE number distributions closely, while the distribution for the first peak ion can be well fitted by a Gaussian, the distribution for the second peak ion is highly asymmetric. It has a long tail towards lower N_e although the high N_e part can be fitted by a Gaussian (dashed curve) with a peak at $N_e = 369$. The SE number distribution for the third peak ion also shows the same characteristic features. The distribution consists of a Gaussian at $N_e = 553$ and a long tail towards lower N_e. The origin of the Gaussian part and the tail part can be explained by the following: The Gaussian part corresponds to the SE's produced by the ions passing through the channel just below the surface (trajectory $2A$ shown in Fig. 5). If there are additional atomic layers on the terrace (trajectory $2B$), the escape probability of the SE's excited by the subsurface channeled ions inside the crystal becomes smaller because the electrons have to travel longer distances than that for the SE's produced by the trajectory $2A$ ions. This results in smaller SE yield and this is the origin of the tail. In fact, a number of pyramidal hillocks like the inset of Fig. 5 were observed on the SnTe(001) surface with atomic force microscopy [14].

The average path length of the trajectory $2A$ ions outside the crystal is the same as that for the first peak ions (see the inset of Fig. 5). Therefore, the average number of SE's produced by the trajectory $2A$ ion outside the crystal is equal to the number of SE's produced by the first peak ion. The dif-

ference ΔN_{12} between the SE yield induced by the first peak ion ($\gamma_1 = 183$) and that for the trajectory $2A$ ion ($N_e = 369$) corresponds to the SE's created by the subsurface channeled ions traveling through the channel just below the surface for one wavelength. If the present explanation is correct, the peak SE number of the Gaussian part for the third peak ion can be estimated as $\gamma_1 + 2\Delta N_{12}$ because the third peak ions travel, on average, for two wavelengths of the channeling motion inside the crystal. The estimated SE yield, $183 + 2 \times (369 - 183) = 555$, is in good agreement with the observed result $N_e = 553$, indicating that the present explanation is appropriate.

Having determined the number of SE's emitted by the subsurface channeled ion, we can address the escape process. The number of electrons excited over the vacuum level by the subsurface channeled ion inside the crystal can be estimated using the calculated SE production rate inside the crystal, which is shown in Fig. 4. The calculated number of electrons excited during one wavelength of the channeling trajectory is 2.4 times larger than that for the first peak ion, while the observed ratio $\Delta N_{12}/\gamma_1$ is $186/183 = 1.02$. Thus, the escape probability of the electrons produced in the subsurface channel is estimated to be $1.02/2.4 \approx 0.42$. It should be noted that the calculation shows that the bulk-plasmon-assisted process is dominant ($\sim 75\%$) in the subsurface channel.

The escape probability is a product of the transport probability $f(x,E_i)$ and the transmission probability $p(E_i)$ to penetrate through the surface barrier, where E_i is the kinetic energy inside the solid and x is the distance below the surface. In a simple model, the transport process is described using a mean free path L, $f(x,E_i) = \exp(-x/L)$, and the transmission probability is given by $p(E_i) = 1 - W/E_i$ for $E_i > W$, where W is the surface-barrier height [15] ($W = 4.3$ eV for SnTe [16]). Because the dominant SE process is the bulk-plasmon-assisted process, we can use $E_i = 14$ eV, which is the typical energy of the SE's produced by decay of bulk plasmons. These values lead to $p = 0.69$ and the transport probability $f(x,E_i) = \exp(-x/L)$ is estimated to be $0.42/0.69 = 0.61$. Using $x = 0.315$ nm [interplanar distance for SnTe(001)], the mean free path L is estimated to be 0.64 nm. The obtained mean free path agrees with the escape depth for Auger electrons of a few tens eV [17].

In a very recent study by Lemmel *et al.* [18], a similar measurement was performed for the SE yield induced by slow multicharged ions reflected from Au(111) at grazing incidence. They demonstrated the suppression of KEE using the specular reflection. The subsurface channeled ions were rejected by choosing the ions reflected at the exact specular angle. However, a small contribution of KEE could not be eliminated, which was ascribed to the contamination of the subsurface channeled ions. Here, we have shown that the specific trajectories of the subsurface channeled ions can be completely selected choosing both the scattering angle and energy of the reflected ions.

IV. CONCLUSION

We have presented a separate observation of the above- and below-surface SE production processes in ion-surface interactions at grazing incidence. The position-dependent SE production rate at the SnTe(001) surface for 2-MeV He^{2+} is found to be about four times larger than that for 0.5-MeV H^+, indicating that the SE production rate is proportional to q_{eff}^2. The below-surface SE production process is studied utilizing the subsurface channeling. The number distribution of the SE's induced by the subsurface channeled ions consists of two components, i.e., a well-defined Gaussian-like peak and a long tail towards lower SE numbers. The peak corresponds to the ion channel through a subsurface channel just below the surface and the tail corresponds to the ions passing through deeper channels. Analyzing the yield of the former one, the escape probability of the SE's produced in the subsurface channel just below the surface is estimated to be ~ 0.4. This escape probability can be explained by a simple model for transport and transmission processes with a mean free path $L \approx 0.6$ nm.

ACKNOWLEDGMENT

We are grateful to the members of the Department of Nuclear Engineering at Kyoto University for the use of the Tandetron accelerator.

[1] See, for example, M. Rösler and W. Brauer, in *Particle Induced Electron Emission I*, edited by G. Hohler and E. A. Niekisch, Springer Tracts in Modern Physics Vol. 122 (Springer, Heidelberg, 1991), p. 1.

[2] See, for example, D. Hasselkamp, in *Particle Induced Electron Emission II*, edited by G. Hohler and E. A. Niekisch, Springer Tracts in Modern Physics Vol. 23 (Springer, Heidelberg, 1991), p. 1.

[3] R. A. Baragiola, E. V. Alonso, J. Ferron, and A. Oliva-Florio, Surf. Sci. **90**, 240 (1979).

[4] K. Kimura, S. Ooki, G. Andou, K. Nakajima, and M. Mannami, Phys. Rev. A **58**, 1282 (1998).

[5] K. Kimura, G. Andou, and K. Nakajima, Phys. Rev. Lett. **81**, 5438 (1998).

[6] K. Kimura, M. Hasegawa, Y. Fujii, M. Suzuki, Y. Susuki, and M. Mannami, Nucl. Instrum. Methods Phys. Res. B **33**, 358 (1988).

[7] B. Monart, Ph.D. thesis, Paris Sud University (1988), IPNO-T-88-01.

[8] M. Hasegawa, K. Kimura, Y. Fujii, M. Suzuki, Y. Susuki, and M. Mannami, Nucl. Instrum. Methods Phys. Res. B **83**, 334 (1988).

[9] M. Fritz, K. Kimura, H. Kuroda, and M. Mannami, Phys. Rev. A **54**, 3139 (1996).

[10] Y. Fujii, S. Fujiwara, K. Kimura, and M. Mannami, Nucl. Instrum. Methods Phys. Res. B **58**, 18 (1991).

[11] J. F. Ziegler, J. P. Biersack, and U. Littmark, in *The Stopping and Range of Ions in Matter*, edited by J. F. Ziegler (Perga-

mon, New York, 1985), Vol. 1.
[12] P. M. Echenique and J. B. Pendry, J. Phys. C **8**, 2936 (1975).
[13] R. Kawai, N. Itoh, and Y. H. Ohtsuki, Surf. Sci. **114**, 137 (1982).
[14] K. Narumi, Y. Fujii, K. Kimura, M. Mannami, and H. Hara, Surf. Sci. **303**, 187 (1994).
[15] M. S. Chung and T. E. Everhart, J. Appl. Phys. **45**, 707 (1974).
[16] I. Abbati, L. Braicovich, and B. De Michelis, J. Phys. C **7**, 3661 (1974).
[17] P. W. Palmberg, Anal. Chem. **45**, 549A (1973).
[18] C. Lemell, J. Stöckl, J. Burgdörfer, G. Betz, H. P. Winter, and F. Aumayr, Phys. Rev. Lett. **81**, 1965 (1998).